ORIGINAL ARTICLE

Open Access

Check for updates

The first 30 min hidden aftershocks of the 2022 September 17, M_L 6.4, Guanshan, Taiwan earthquake and its seismological implications

Bor-Shouh Huang[1*] , Chin-Shang Ku[1], Chin-Jen Lin[1], Shiann-Jong Lee[1], Yen-Ling Eileen Chen[2], Juen-Shi Jiang[2] and Wei-Fang Sun[3]

Abstract

The first 30 min of the aftershock sequence following the 2022 September 17, M_L 6.4, Guanshan, Taiwan earthquake is investigated by the back-projection (BP) method. Based on the Automatic Gain Control (AGC) to process individual earthquake record and sort waveforms by epicentral distance, 80 events are identified near the Guanshan earthquake epicenter to verify its temporal variation. However, most of these events cannot clearly image by the BP method to determine its spatial locations for its small amplitude and short time separation. In total, 29 aftershocks are imaged by this study to identify its spatial locations during this time period. The relocated events are compared with the Central Weather Bureau (CWB) rapid report catalogue. Only 5 events have been reported by the CWB rapid report catalogue. These unreported hidden aftershocks are identified to distribute surrounding the epicenter and extended to the east. This extracted information of hidden aftershocks is crucial for assessing the potential for future large aftershocks and estimating the associated seismic hazards in a given region, and provide extra message to evaluate the source physics in general.

Key Points

1. Propose and verify earthquake location using the back-projection method.
2. Discover 29 hidden events with 30 min after the Guanshan earthquake.
3. Provide extra information to study following large aftershocks and to estimate its associated seismic hazards.

Keywords Guanshan earthquake, Hidden aftershocks, Back-projection, Automatic gain control, Central Weather Bureau

*Correspondence:
Bor-Shouh Huang
hwbs@earth.sinica.edu.tw
[1] Institute of Earth Sciences, Academia Sinica, 1-55, Nankang, P.O. BOX, Taipei 115, Taiwan
[2] Seismological Center, Central Weather Administration, Taipei, Taiwan
[3] Department of Geosciences, National Taiwan University, Taipei, Taiwan

1 Introduction

In September 2022, an earthquake sequence occurred in the Eastern Taiwan. There were four earthquakes with magnitudes greater than 6 in this sequence (Fig. 1a). Among them, the Guanshan earthquake was the first large event with a magnitude of M_L 6.4 occurred on September 17, 2022. The biggest Chihshang earthquake with

Huang *et al. Terrestrial, Atmospheric and Oceanic Sciences* (2024) 35:1

Page 2 of 14

a magnitude of M_L 6.8 occurred on September 18, 2022 following. Both events have the intense shocks, causing surface ruptures and multiple disasters. Although the eastern region of Taiwan is prone to earthquakes, the location where this earthquake sequence occurred is situated in an area with relatively low seismic activity (Lee et al. 2023). According to early survey reports (https://fault.gsmma.gov.tw/Reports/More/63cc5a4b20 20403d9f79d3c33a7aba0c), the earthquake processes and source rupture behavior of this earthquake sequence are unique. Following a major earthquake, usually, large number of aftershocks are always triggered in the epicentral area within a short period of time. The small earthquakes that occur immediately after the mainshock (for example of the first 30 min) and are located near or within the ruptured area of the earthquake can provide significant information to explore the earthquake source physics and rupture characteristics. In Taiwan, both early warning strong motion network and regional seismic network usually play the role in detecting the aftershocks and monitor earthquake sequence. The early warning strong motion network always reports large event in first time. However, both aftershocks directly masked by the main shock's coda wave or aftershocks with very small magnitudes, are often difficult to be detected by both seismic networks. The events that were missed to report are referred to as "hidden events" in this study and the same as Kiser and Ishii (2013). To retrieve those hidden aftershocks, the deployment of a high-density temporary seismic network, utilizing highly sensitive seismometers and complete coverage of the earthquake source area is expected.

In this study, we aim to investigate the aftershocks of the Guanshan earthquake. As it is the first large event of this earthquake sequence, the identification of aftershocks is not yet affected by other large earthquakes, which greatly reduces the uncertainty of the aftershock study. The earthquake rapid report catalog published by the Central Weather Bureau (CWB) mainly relied the early warning strong motion network for location determination (https://www.cwa.gov.tw/V8/C/E/index.html). The complete event catalog is updated using data from the Central Weather Bureau Seismographic Network (CWBSN), a regional network, and added more small events. The final event catalog of CWBSN will be checked manually and usually delayed several months. However,

there was no extra temporary seismic stations set up in the eastern region of Taiwan at the moment of the Guanshan earthquake occurred, it can be expected that smaller aftershocks will not be effectively detected and reported. In the study, we will examine the continuous recordings of the Taiwan Strong Motion Instrumentation Network (TSMIP), a dense seismic network originally designed for earthquake engineering applications, to extract earthquake data for aftershock analysis. We hope to locate all aftershocks of the first 30 min and retrieve small events that were not included in the CWB rapid report catalog (https://scweb.cwa.gov.tw/zh-tw/earthquake/data/). By using newly developed methods to analyze the recorded high spatial-density earthquake data for earthquakes in or near the source area, we are able to locate more hidden aftershocks lost by the CWB rapid report catalog. New messages from these small earthquakes enable us to discuss the source processes of the Guanshan earthquake, as well as to explore characteristics of earthquakes which occurred in an aseismic zone.

1.1 Regional tectonics and seismic activities in the eastern Taiwan

Taiwan is located at the collisional boundary between the Eurasian Plate and the Philippine Sea Plate. The Philippine Sea Plate is moving relative to the Eurasian Plate towards the northwest direction. The fault system in eastern Taiwan is influenced by the oblique collision and strong convergence between two blocks. The dominate fault of this region is named as the Longitudinal Valley fault, it connects the two arc-trench systems of the Ryukyu and Manila trenches. The eastern region of Taiwan is known as a high seismic risk, and has experienced multiple disastrous earthquakes in history (Shyu et al. 2007; Lee et al. 2008; Huang et al. 2009; Mozziconacci 2013a; Wen et al. 2019). The Hualien-Taitung Valley was hit by several strong earthquakes in 1951, with the largest two earthquakes reaching a magnitude of 7.3 on the Richter scale. The 1951 earthquake series have caused serious damage in the source area. Over the past 70 years, this region has several earthquake sequences occurred with damage reports (https://tec.earth.sinica.edu.tw/index. php). On 2022, the Eastern Taiwan earthquake sequence occurred in the southern part of the Hualien-Taitung Valley (Fig. 1a). The source area of this earthquake sequence is located at an active hidden fault zone in the western

(See figure on next page.)
Fig. 1 a Schematic geological map of the source region and four major events of this earthquake sequence with magnitude greater than 6 (modified from Lee et al. 2008). Brown circle indicates the Guanshan earthquake, blue circle indicates the Chishang earthquake and two yellow circles indicate other reported events. **b** The recorded events of the Chishang region by CWNSN from 2022/09/01 to 2022/09/30. The event magnitudes are scaled by the size of event symbols (circle) from magnitude 6 to 1. Event depths are scaled by the color bar listed below. Both Guanshan and Chishang events are indicated as blue star and circle, respectively
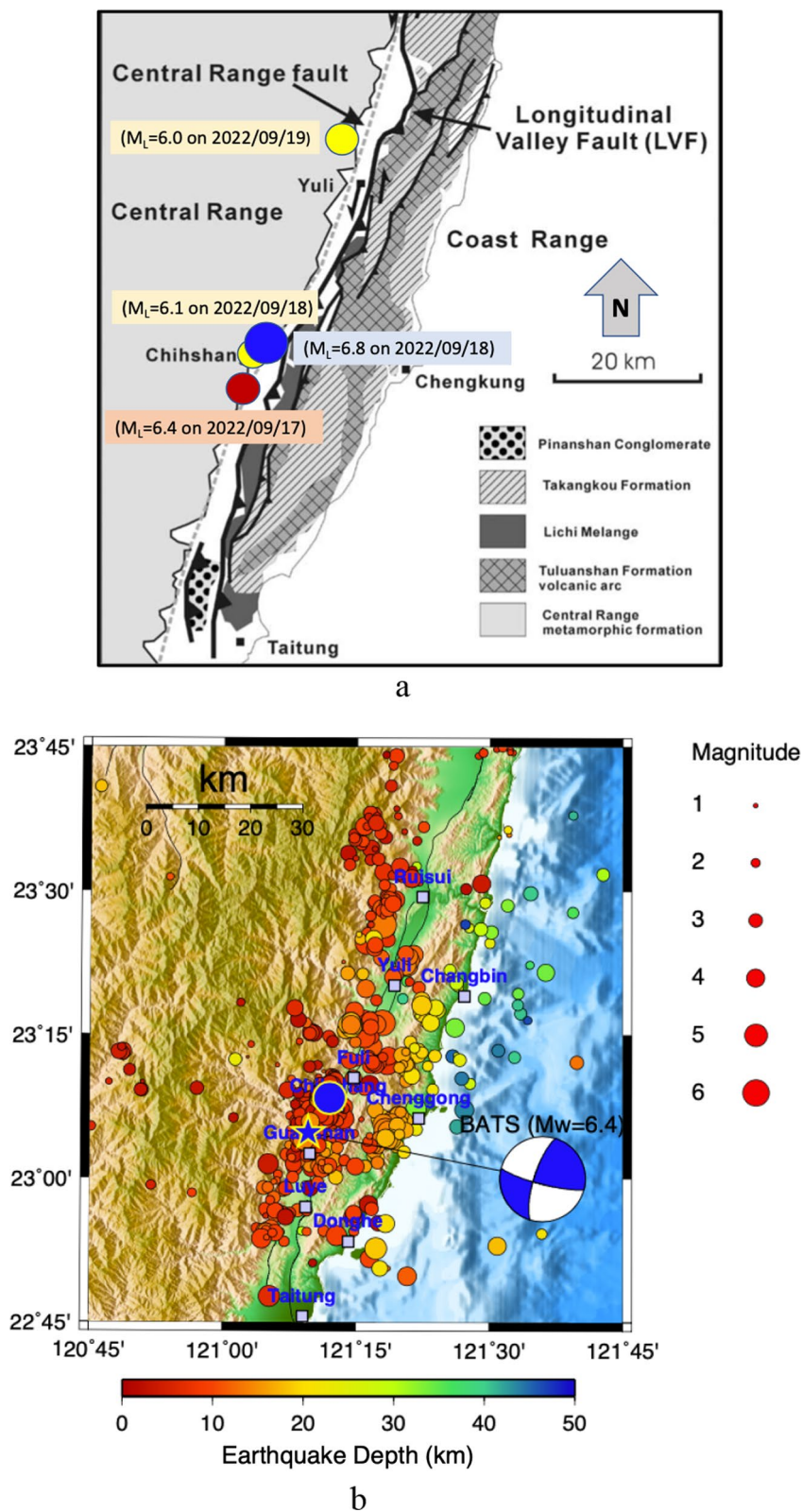
Fig. 1 (See legend on previous page.)

Huang *et al. Terrestrial, Atmospheric and Oceanic Sciences* (2024) 35:1

Page 4 of 14

side of the Hualien-Taitung Valley suture zone near the Central Mountain Range. This fault system is adjacent to the Longitudinal Valley fault in the coastal mountain range, and seismic activities between the two fault systems are often linked (Shyu et al. 2006; Mozziconacci 2013b; Lee et al. 2023). Referring to the distribution of long-term earthquake activity in Taiwan, this earthquake sequence occurred in an area with relatively low seismicity region.

1.2 Seismic observations

On September 17th, 2022, an earthquake occurred at 21:47 local time, with a magnitude of M_L 6.4. The epicenter was close to Guanshan in Taitung, at latitude 23.08°N and longitude 121.16°E. On September 18th, 2022, the earthquake occurred at 14:44 local time, with a magnitude of M_L 6.8. The epicenter was close to Chishang in Taitung, at latitude 23.14°N and longitude 121.2°E. In Taiwan, the reporting of felt earthquakes and the warning of large earthquakes is carried out by the early warning strong motion network of CWB (https://www.cwa.gov.tw/V8/E/E/index.html). Till the end of September, this earthquake monitoring network detected a total of 207 felt earthquakes during the monitoring of the 2022 Eastern Taiwan earthquake sequence. The temporal distribution of the earthquakes was dominated by the Guanshan (foreshock) and Chishang (mainshock) earthquakes, each showing a clear mainshock-aftershock relationship (Lee et al. 2023). After the Chishang earthquake, aftershocks continued to occur towards the north, eventually extending to the vicinity of Ruisui in Hualien (Fig. 1b). According to the reported moment tensor solutions (https://tecdc.earth.sinica.edu.tw/FM/AutoBATS), the source mechanisms of both events are similar. The possible fault plane is oriented in a north-northeast to south-southwest direction, with a high angle and westward dip, and is dominated by left-lateral slip (Fig. 1). The maximum seismic intensity of the two earthquakes reached level 6 in various parts of Taiwan, and the depth of both earthquakes was only about 7 km, which is considered extremely shallow.

1.3 Data collected from TSMIP

The geological environment in Taiwan is complex and diverse. In order to capture the regional seismic characteristics of large earthquakes, from early 1990, the CWB has continuously installed 737 free-field strong motion sensors in densely populated plain areas and named as TSMIP. Its main mission is for engineering applications, to investigate site effects caused by local geological differences in Taiwan due to earthquake waves, and to establish regulations to achieve the goal of earthquake resistance and disaster reduction. Its secondary mission

is for seismological applications, to support earthquake research in related fields by studying path effects of wave propagation and source effects of large earthquakes, including the source size and rupture process. Since 2018, the CWB has upgraded part of TSMIP stations to continuous recording and real-time transmission of data to provide earthquake intensity reports and plan for emergency response needs following future major earthquakes. After the upgrade, a strong motion network with continuous recording has been established. Currently, there are about 400 free-field strong-motion stations, mainly distributed in the Taiwan plain and metropolitan areas (https://gdmsn.cwa.gov.tw/network_tsmip.php).

During the 2022 eastern Taiwan earthquake sequence, the TSMIP stations continuously recorded the events and the network was fully operational. Figure 2 displays the seismic stations surrounding the epicenter of the Guanshan earthquake and the vertical component seismograms for seismic stations within 100 km epicenter distances. The high spatial density of stations near the source region and the resulting high-resolution seismograms enable a detailed examination of the Guanshan earthquake and its aftershocks. This study focuses on enhancing aftershock signals and relocating events using an array stacking approach, which eliminates the need for phase picking of emergent first arrivals of small events. The methods of analysis proposed will be explained in the next section.

2 Methods
2.1 Automatic gain control: signal enhancement for low amplitude aftershocks

Automatic gain control (AGC) is one of the most common gain recovery methods used in seismic signal processing. In this study, the concept of AGC will be applied to process earthquake multiple event seismograms, increase the strength of aftershock signals to identify the timing of aftershocks and perform location estimation. AGC is a type of limited output that uses a combination of linear amplification and compression amplification to adjust the output of the original signal. When a weak signal is input, the seismic signal is linearly amplified to ensure the output signal strength. When the input signal reaches a certain strength, the compression of the seismic signal is activated, causing the output amplitude to decrease.

In this study, we proposed the Root mean square (rms) amplitude automatic gain control (or named as rms amplitude AGC) for signal enhance. This method is one of the most commonly used types of gain control (Gadallah and Fisher 2005, 2009). The rms amplitude AGC gain function is based on the rms amplitude of the input signal within a specified time window. The gain function is
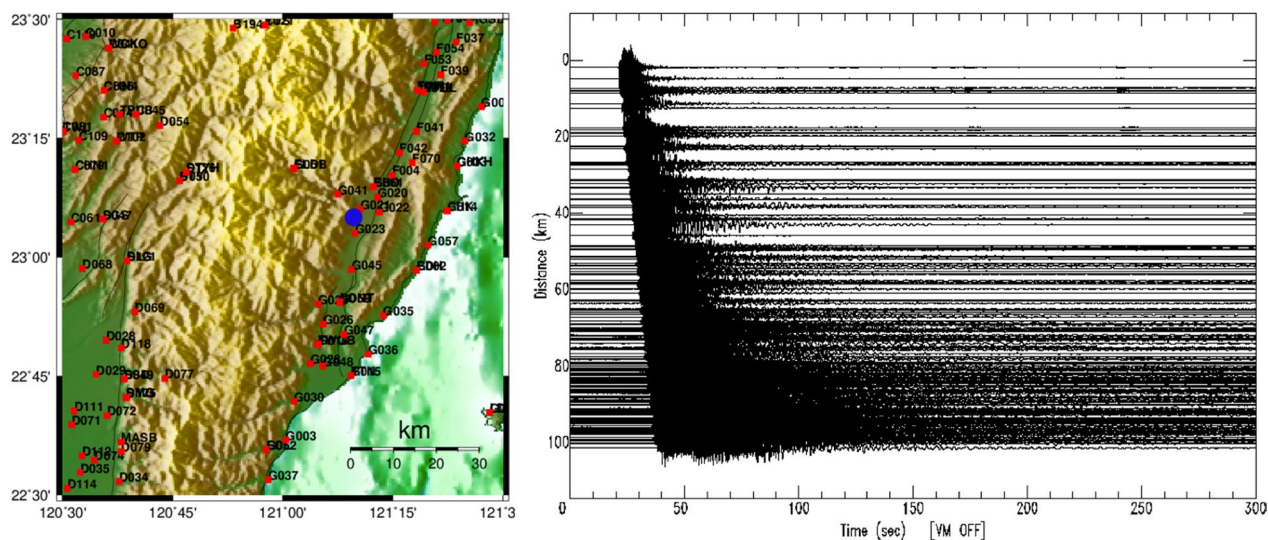
Fig. 2 a The selected stations of TSMIP recorded the Guanshan earthquake with epicentral distance less than 100 km. **b** Vertical array waveforms plotted by epicentral distances

calculated as follows: first, the input seismic waveform is divided into fixed time windows, and the square of the amplitude of each sample in the time window is calculated. Second, the average of these values is calculated, and the square root is taken. This is defined as the rms amplitude of the time window. The ratio of the desired rms amplitude (for example, a value of 2000) to the actual rms value is specified as the value of the gain function at the center of the time window. Therefore, the scaling function g(t) at the center of the time window is given by the following equation:
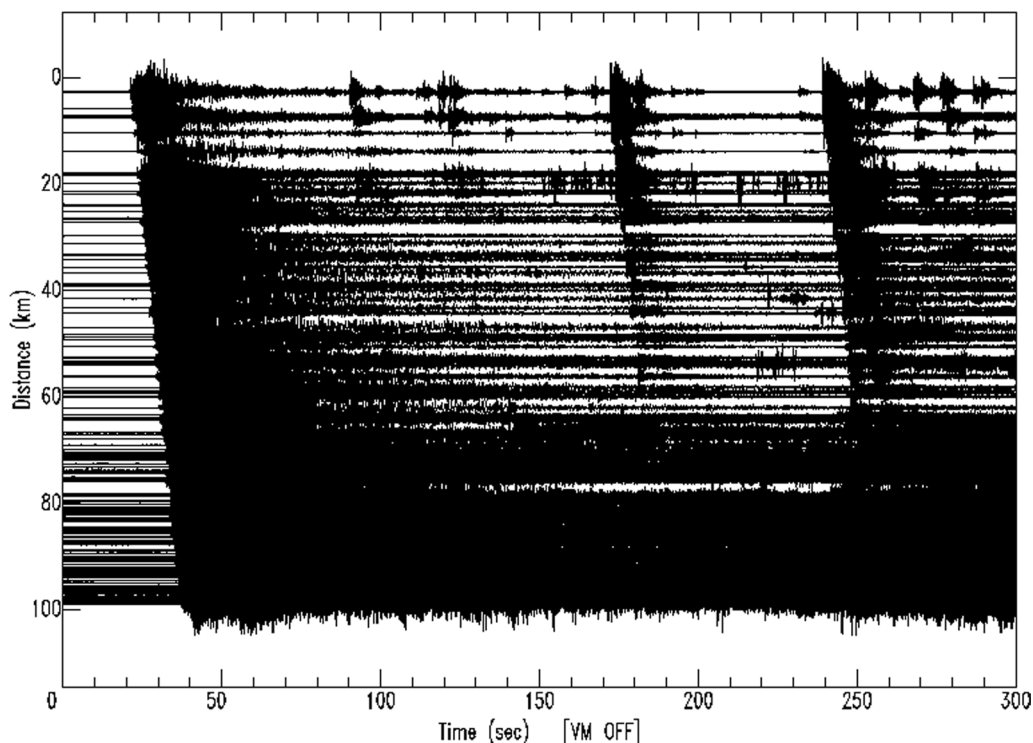

Fig. 3 The same seismic waveforms of Fig. 2b processed by the AGC algorism to enhance aftershocks. Each trace is scaled to the same size in this record section

$$g(t) = \frac{\text{desired rms}}{\sqrt{\frac{1}{N}\sum_{i=1}^{N} x_i^2}}, \qquad (1)$$

where x_i is the amplitude of the input signal at time point i, and N is the number of samples within the window.

To demonstrate the effectiveness of our processing method, this study used the Guanshan earthquake and its aftershock data for the following 300 s as an example, as shown in Fig. 2. The seismic records from the near-source station did not show any clear aftershock signals, and the earthquake catalog from the Central Weather Bureau did not list any located aftershocks also within this 300-s time window. However, after applying the Automatic Gain Control (AGC) method proposed in this study to enhance the aftershock signals, the obtained results are shown in Fig. 3. Comparing the two figures, it is evident that multiple aftershocks near the Guanshan earthquake source occurred within this 300-s time window after the main earthquake, which were not visible in the seismic records without the AGC processing. This example highlights the potential application of the AGC method in detecting hidden aftershocks within a short time window following a major earthquake.

2.2 Back-projection (BP) method: application for earthquake location

The BP method uses a grid search approach to consider all grid points within the model as possible earthquake source locations. The seismic wave travel time differences between each grid point and all seismic stations are calculated using an appropriate velocity model (Ishii et al. 2005). By moving all grid points appropriately to match the seismic wave travel times recorded by the seismic stations, the earthquake wave energies are shifted in time and overlaid to obtain the corresponding peak values. The grid point that produces the highest peak value is identified as the earthquake source through evaluation. The calculation steps can be represented by the following formula:

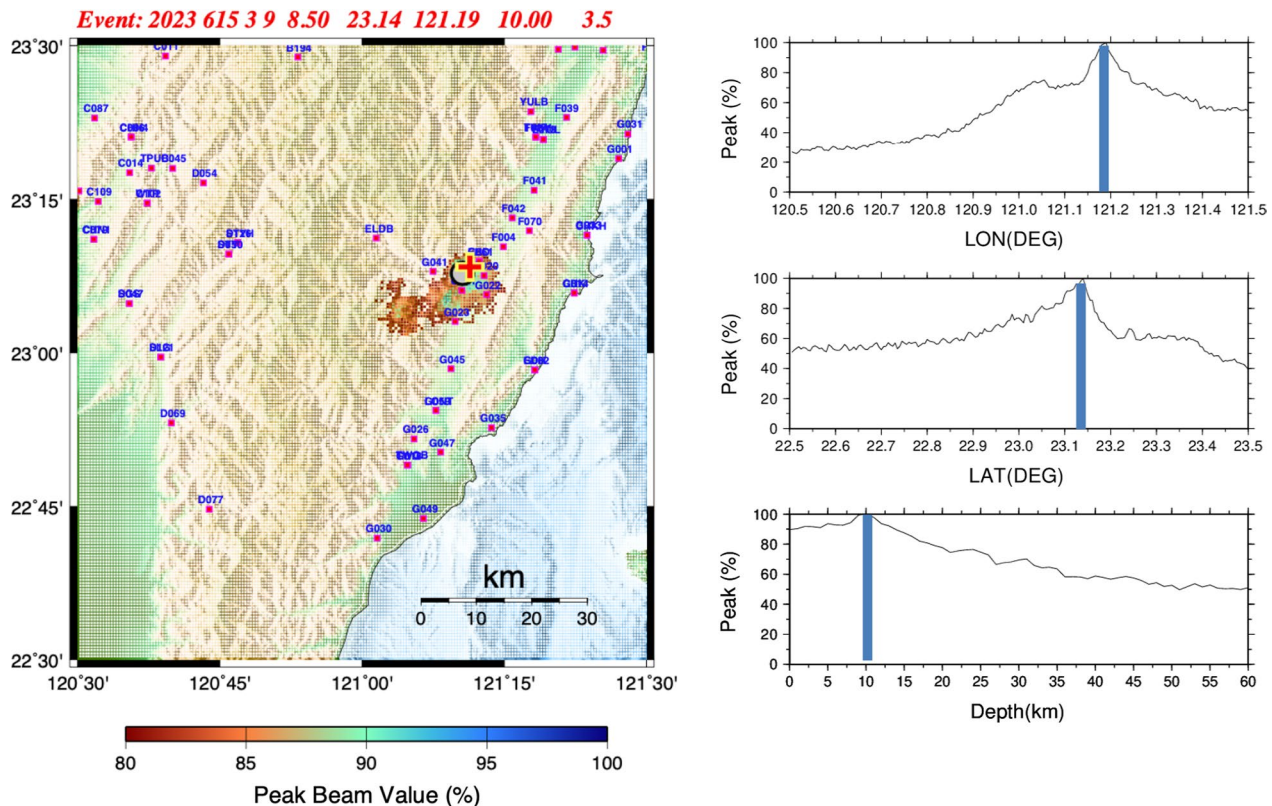$$\text{Stack}_i(t) = \frac{1}{N} \sum_{k=1}^{N} S_k(t - t_{ik}), \qquad (2)$$

Fig. 4 Comparison of event locations reported by the CWB (indicated as circle) and BP (symbol: +). The spatial variation of epicenter in the EW, NS and Vertical components are shown in right panels following the BP method. This is a selected event on eastern Taiwan from CWB rapid catalog (event time: 2023/06/15/03:19:8.5) as an example. Total of 150 TSMIP waveforms with epicentral distances less than 150 km are selected by BP to locate events. The data has been previously processed by 1 Hz low pass filterer to remove incoherence signals

Huang *et al. Terrestrial, Atmospheric and Oceanic Sciences* (2024) 35:1

Page 7 of 14

where $Stack_i(t)$ represents the time series of earthquake waveform energy summed over all seismic stations, N is the number of seismic stations, k is the index of the kth seismic station, $S_k(t)$ is the seismic wave amplitude time series of the kth seismic station, and t_{ik} is the theoretical travel time between index grid point i of the model and the kth seismic station (Ishii et al. 2007). The theoretical travel time used for stacking can be either the travel time of P-waves or S-waves.

To locate an earthquake using the BP method, we need to discretize the earth model into a three-dimensional (3-D) grid. Assuming the true location of the earthquake source is within the 3-D grid. As a sample, we calculate the predicted travel times from location of a selected grid point within the model to each seismic station. We then time-shift the seismic records based on predicted travel times, and stack all seismic records for this grid point. Each grid point within the model is considered a potential earthquake source and the same calculations are repeated for each point of the model. If the grid point is the true hypocenter, the arrival times will align after time shifting, resulting in a constructive stack on the seismic record. For other non-source grid points, they will not align, and the stack out of phase. This repetitive process generates a 4-D BP image that includes the time history of the stack amplitude at each potential hypocenter within the search 3-D volume. Finally, the earthquake hypocenter location and origin time are represented by the time point of maximum amplitude at the corresponding grid point. A unique feature of the BP method is
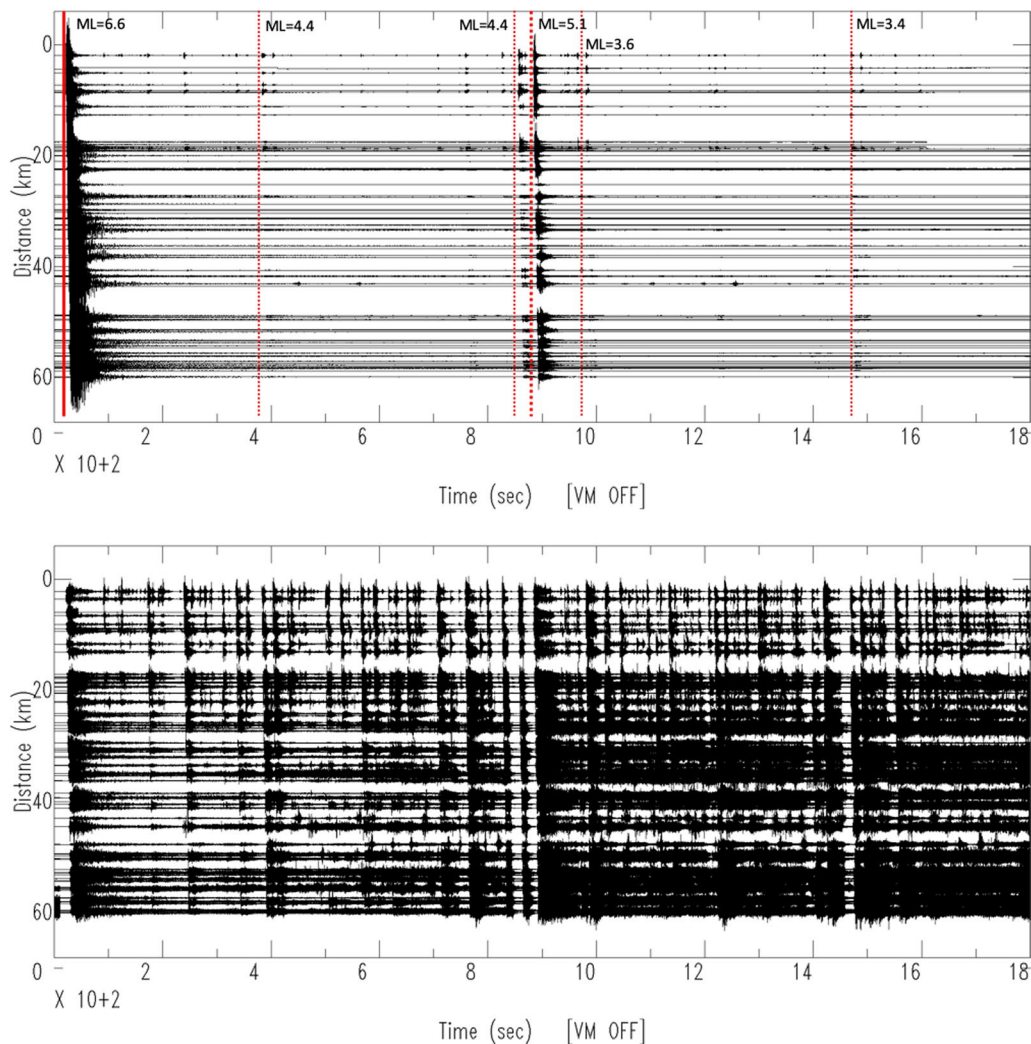

Fig. 5 **a** 30-min vertical component continuous data after the M_L 6.4, Guanshan earthquake collected from the TSMIP stations with epicentral distances less than 60 km. Vertical dashed lines (red) denote original time of aftershocks reported by the CWB rapid catalog. **b** The same network vertical-component waveforms on upper panel processed by AGC (10 s time window) to modulate aftershock amplitudes. Small events with similar alinement of mainshock are seen in this profile. It indicates all events near the epicenter and considered as near source aftershocks
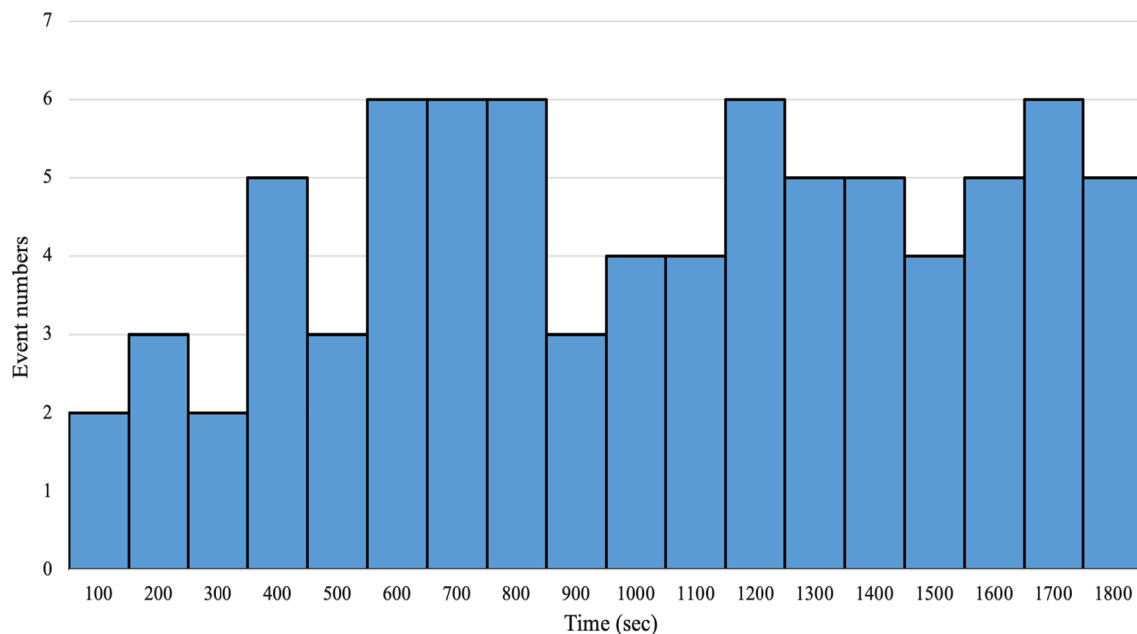
Fig. 6 The counted number with time plot (The N-T chart) of the first 30 minters minutes aftershocks of the 2022 September 17, M_L 6.4, Guanshan earthquake

that there is no need to pick arrival times for the seismic records during the earthquake location process.

In this study, we have developed a suitable program based on above procedure. The earthquake location calculation is performed by directly stacking seismic records from the TSMIP network with a dense array configuration. A 1-D regional model of Taiwan (Roecker et al. 1987) and a lateral homogeneous raytracing method (Huang 1996) are selected for the predicted travel times used in this study. Example for a medium magnitude event in the eastern Taiwan is shown in Fig. 4 (left panel), and the corresponding resolution (stacked energy) checks on the right.
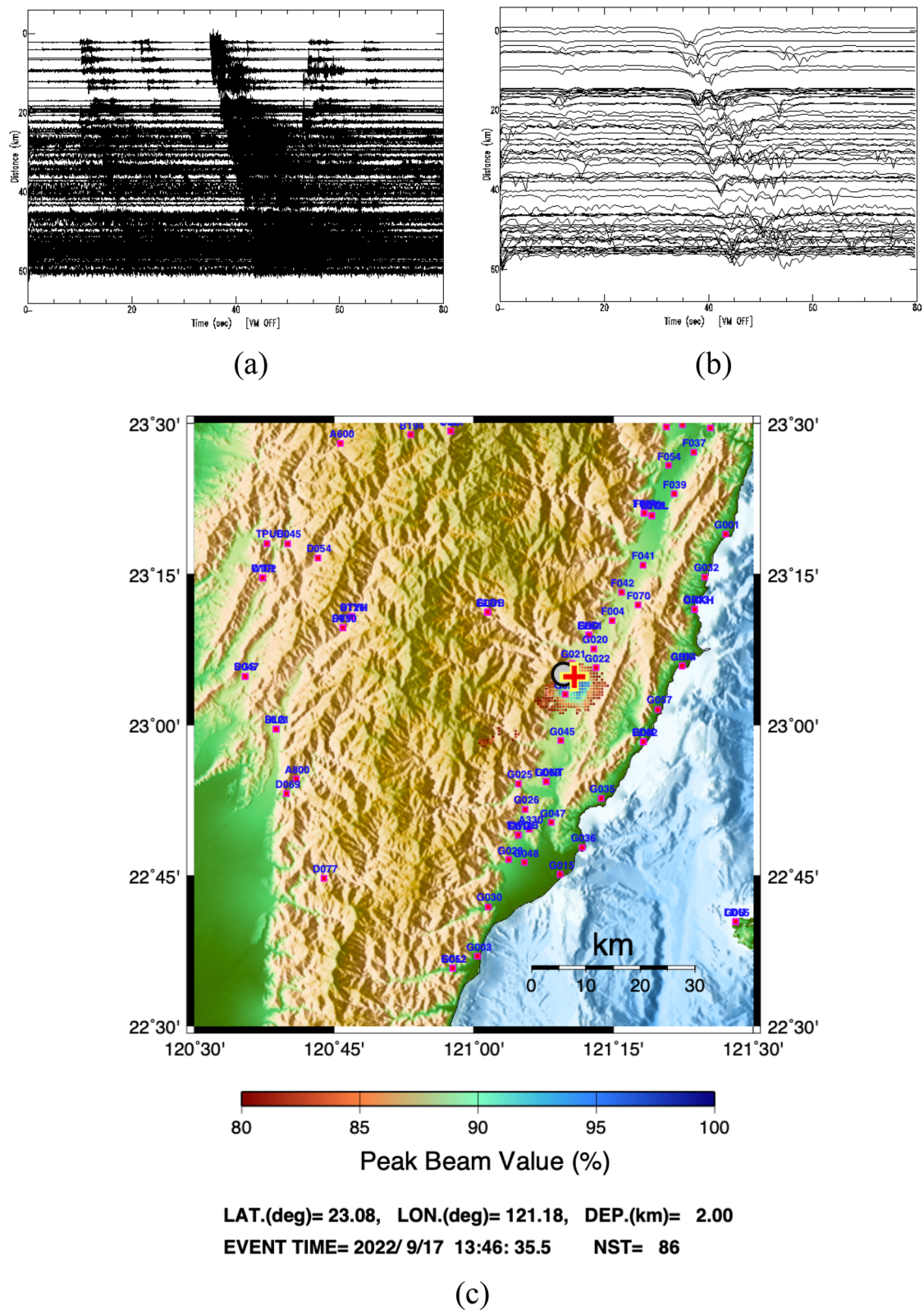
2.3 Analysis and results

To effectively locate earthquakes, we selected data with a high signal-to-noise ratio from nearby stations of the Guanshan earthquake epicenter (as shown in Fig. 2) for analysis. In this study, we selected data from TSMIP seismic station within 60 km of epicentral distance. In total, 87 vertical component seismograms have been selected to use in this study. For each station, a total of 30-min time trace (including the Guanshan earthquake) was extracted and plotted on a figure based on the epicentral distance of the Guanshan earthquake, as shown in Fig. 5a. Although several low-amplitude aftershock signals have showed in selected stations, however, the CWB fast report catalogue only identified and marked five

aftershocks during this time period on their rapid report website.

In this study, AGC is used in data processing to improve the visibility of aftershocks in which attenuation or spherical divergence has caused amplitude decay. The rms AGC is used for amplitude equalization. It gives a measurement of the overall absolute amplitude in the window, both as positive and as negative values. To perform the automatic detection, a fixed gate length is necessary. After several trying, we selected 10 s for this case. Corresponded to Fig. 5a, the processed AGC Plots of seismograms is shown in Fig. 5b. It shows that each trace has similar time moveout, it indicates those events are closer to the epicenter of Guanshan earthquake. In total, 80 events have identified in this plot as events near the M_L 6.4 Guanshan event. The counted event number with time (N-T plot) have been summarized as Fig. 6.

In this study, the method to locate aftershock for this M_L 6.4 Guanshan earthquake will be the BP method proposed in this study. It will be carried out through the energy superposition of seismograms without individual picking the arrival times of seismic waves. The total aftershock location processes will be based on 30-min seismic data and processed with AGC to enhance weak signals (Fig. 5b). We extract the common time window of seismograms containing aftershock signals for further earthquake location. Taking Fig. 7 as an example, we selected the waveform data from 300 to 380 s in Fig. 5b (as shown in Fig. 7a) for the following

(a)

(b)

(c)

LAT.(deg)= 23.08,   LON.(deg)= 121.18,   DEP.(km)= 2.00
EVENT TIME= 2022/ 9/17 13:46: 35.5   NST= 86

Fig. 7 a AGC enhanced waveforms of event 4 (Table 1), (**b**) enveloped waveforms and (**c**). the BP location report of this study. NST: the number of stations (vertical component waveforms) selected to relocate this event
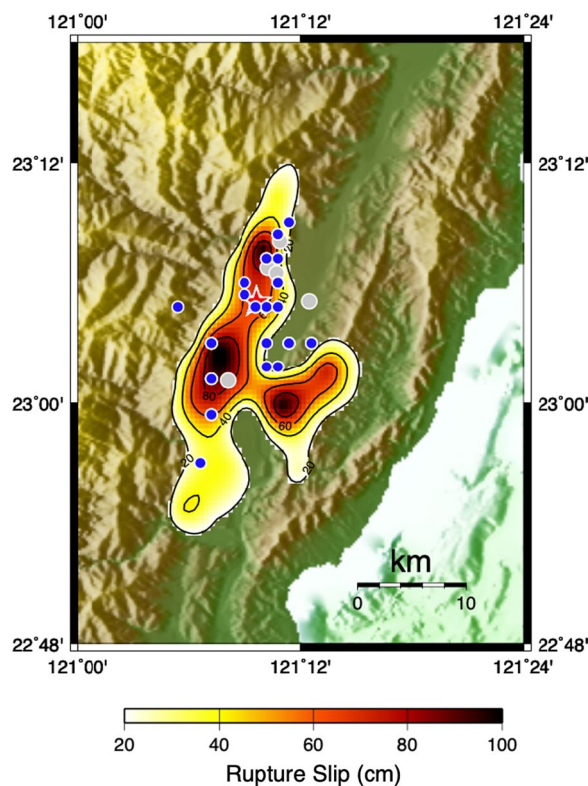
Fig. 8 The located events of this study (small blue circle symbols), CWB reported events (medium gray circle symbols) and source rupture slip distribution (colored contours in unit of centimeter) of the Guanshan earthquake reported by Lee et al. (2023). The CWB reported Guanshan earthquake is plotted as the symbol of big red star

earthquake location determination. To ensure the stability of the superposition results, we converted the selected waveform data into its envelope forms to provide time traces as shown in Fig. 7b. By performing the energy superposition computation using Eq. (2) of this study, we ultimately obtained the spatial coordinates and origin time of the located aftershock, as shown in Fig. 7c. The same procedure will be applied to all distinguishable time windows of aftershocks within this 30-min period. However, most of the time windows of aftershocks are too short to complete stable image superposition. In the end, a total of 29 aftershocks have located and are all plotted in Fig. 8, with their corresponding source parameters listed in Table 1. The results show that major aftershocks are distributed on the north and south sides of the epicenter, with a small number of them distributed in the eastern side.

3 Discussion and conclusions

As shown in Fig. 8, the aftershocks determined in this study (29 events) presents more detailed spatial distribution than that determined by CWB (5 events)

within the same time period. It indicated that the M_L 6.4 Guanshan earthquake has triggered a series of aftershocks in the source region. The earthquake locating process of CWB primarily involves extracting the arrival times of seismic waves to simplify the seismic data. It then goes through validated and widely used computer locating programs such as HYPO71 (Lee and Lahr 1975; Lee et al. 2003), HYPOINVERSE (Klein 1978, 2003), HYPOELLIPSE (Lahr 1989, 2003), etc., to perform data inversion and confirm the epicenter location. Although the locating system of CWB adapts to regional variations and optimizes rapid reporting operations by moderately modifying existing computer locating programs, the fundamental approach still requests picking the arrival times of seismic waves and then locating the earthquake. Above earthquake location methods relying on first arrival picking is challenging for small events with low signal-to-noise ratio or multiple events occurred in a short time period.

To address this issue, we used an alternative procedure to explore, it based on the idea of migrating the energy of an earthquake back into its source position by stacking along theoretical travel-time curves. We selected also the TSMIP data which is a dense seismic array designed for seismic hazard assessment purposes and does not used for event location. In this study, employed the BP method which is a technique commonly used to image seismic sources (Ishii et al. 2005; Meng et al. 2011; Beskardes et al. 2018). This method utilizes the recorded seismic waveforms from multiple stations and calculates the correlation between each station and potential source locations. By scanning the entire study area, this method is able to identify hidden aftershocks that may have been missed by conventional methods. In this study, we revised this method with AGC to enhance buried signals to retrieve the early aftershocks of the 2022 September 17, Guanshan Taiwan earthquake. The findings of the study reveal that the BP method successfully detects and locates a significant number of hidden aftershocks that were not previously identified. The identified aftershocks provide valuable insights into the fault geometries and seismic activity in the region following the main earthquake. It provides an opportunity to view the evolution this earthquake sequence.

The overlaid beneath Fig. 8 is the coseismic slip distribution of the Guanshan earthquake inferred through joint inversion of multiple geophysical data by Lee et al. (2023). The hidden earthquake distribution determined in this study is consistent with the main slip distribution of the Guanshan earthquake. According to the study by Lee et al. (2023), the main rupture of this earthquake sequence mainly occurred on a west-dipping fault and

Table 1 Relocated events of this study (#01 is the M_L 6.4 Guanshan earthquake)

#	Year	m	d	h	mn	sec	lat	lon	dep	DLEQ[a]
01	2022	09	17	13	41	29.0	23.03	121.18	00.00	
02	2022	09	17	13	43	54.0	23.08	121.09	06.00	+
03	2022	09	17	13	44	59.0	23.05	121.21	14.00	+
04	2022	09	17	13	46	35.5	23.08	121.18	02.00	+
05	2022	09	17	13	47	23.5	23.03	121.17	12.00	+
06	2022	09	17	13	47	43.0	23.05	121.19	02.00	+
07	2022	09	17	13	50	25.0	23.10	121.15	07.00	+
08	2022	09	17	13	52	46.5	23.10	121.18	08.00	+
09	2022	09	17	13	53	39.0	23.05	121.17	03.00	+
10	2022	09	17	13	54	45.5	23.05	121.21	15.00	+
11	2022	09	17	13	55	44.5	23.14	121.18	04.00	+
12	2022	09	17	13	57	05.0	23.09	121.15	02.00	+
13	2022	09	17	13	57	20.0	23.10	121.18	08.00	+
14	2022	09	17	13	57	55.0	22.95	121.11	09.00	
15	2022	09	17	13	58	23.0	23.12	121.18	02.00	+
16	2022	09	17	13	59	54.0	23.05	121.19	09.00	+
17	2022	09	17	14	00	48.5	23.10	121.18	08.00	+
18	2022	09	17	14	01	07.0	23.08	121.17	13.00	+
19	2022	09	17	14	01	18.0	23.15	121.19	13.00	+
20	2022	09	17	14	01	36.0	23.12	121.18	07.00	
21	2022	09	17	14	02	37.5	23.14	121.18	07.00	+
22	2022	09	17	14	04	17.0	22.99	121.12	10.00	+
23	2022	09	17	14	04	39.0	23.05	121.12	03.00	+
24	2022	09	17	14	05	29.0	23.02	121.12	03.00	+
24	2022	09	17	14	05	47.0	23.12	121.17	07.00	+
26	2022	09	17	14	06	50.5	23.05	121.19	11.00	+
27	2022	09	17	14	06	55.5	23.15	120.98	57.00	
28	2022	09	17	14	07	35.0	23.08	121.18	07.00	+
29	2022	09	17	14	07	47.0	23.08	121.16	13.00	+
30	2022	09	17	14	08	30.5	23.15	120.98	57.00	

[a] DLEQ: Events(+) commonly located by Deep Learning (DL) method (Sun et al. 2023)

its slip originated from the hypocenter and propagated toward the north. The Guanshan earthquake is considered as a foreshock in the earthquake sequence, understanding its detailed aftershock activity may provide an opportunity to insight the subsequent earthquake development. By examining the spatial and temporal distribution of these aftershocks, it may identify statistical patterns that can be used for forecasting purposes (Zhang et al. 2021) and the size distribution, and short-term forecasting of large aftershocks. It has important implications for evaluating seismic hazards (Gulia et al. 2018). However, it is beyond the scope of the initial research of this study.

To validate the performance of the BP method of this study, we compared our results with new location event catalog of this earthquake sequence by Sun et al. (2023) based on an independent dataset of this earthquake sequence. For monitoring micro-seismicity on the creeping Chihshang Fault system and due to the sparse distribution of seismic stations in eastern Taiwan, NTU and IES deployed five broadband stations (red triangles in Fig. 9), the Chihshang seismic network (CSN), in early November 2021 to increase the station coverage. From September to October 2022, SeisBlue (Huang et al. 2023; Kuo-Chen et al. 2022), a deep learning-based seismological data processing platform, detects 6924 earthquakes by using the continuous seismic data from the 9 BATS stations without the CSN data but 14,454 earthquakes by combining the CSN and BATS data. Particularly on 17 September 2022 when the strong Mw 6.5 foreshock occurred, SeisBlue detects about 100 events without the CSN data but over 800 events with it. The earthquake detection ability is greatly improved by the CSN data. The details of the two-month (September to October 2022)
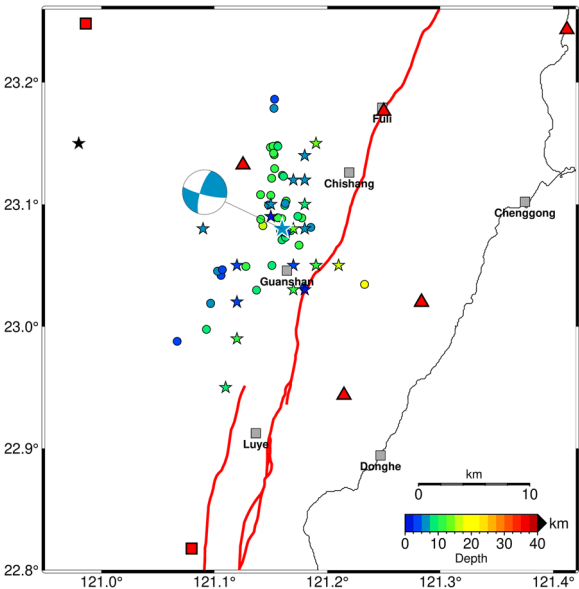
Fig. 9 The 30-min aftershock seismicity right after the 2022-09-17 Guanshan earthquake occurred. The colored circles and starts are events detected by SeisBlue (Sun et al. 2023) and this study, respectively. Red triangles and squares are broadband stations. Gray squares indicated the locations of city or county. Red traces are active faults identified by Central Geological Survey, Taiwan (Lin et al. 2021) and the names of regional faults are referred to Fig. 1a

deep learning-based SeisBlue earthquake catalog of the 2022 Mw 2022 Chihshang earthquake sequence would be described in Sun et al. (2023) included in this special issue. The SeisBlue earthquake catalog contains 43 aftershocks that occurred within 30 min after the Mw 6.5 Guanshan foreshock struck (Fig. 9; Table 2). Those events are located by the program HYPOCENTER (Lienert and Havskov 1995) with a 1-D velocity model by Central Weather Bureau, Taiwan (Chen and Shin 1998). Comparison of the located event number and distribution of epicenter are similar from both BP and the deep learning (DL) location methods. However, it shows some differences in detail. The original times for commonly located events showed several second variations and epicenters from BP method showed lower spatial resolutions than DL method. Both differences can be explained as different earth models are used by BP and DL methods, and the BP method used rough grids to search its epicenter. Furthermore, two events are located on western side of source region as deep events by BP method (Table 1) and do not identified by the DL method (Fig. 9). After checking array observations, it is found that multiple small events are identified on selected seismograms and both hypocenters are mislocated by BP stacking approach.

Table 2 Earthquakes detected by SeisBlue using 14 permanent broadband stations for the first 30 min after the Mw 6.5 Guanshan foreshock occurred

#	Year	m	d	h	mn	sec	lat	lon	dep	BPEQ[a]
01	2022	09	17	13	43	50.1	23.07795	121.15854	07.92	+
02	2022	09	17	13	44	56.9	23.07088	121.15987	09.66	+
03	2022	09	17	13	46	07.8	23.08831	121.15965	10.57	
04	2022	09	17	13	46	33.1	23.07819	121.16427	05.92	+
05	2022	09	17	13	47	20.7	23.08888	121.17744	10.06	+
06	2022	09	17	13	47	40.4	23.07638	121.16339	09.78	+
07	2022	09	17	13	49	18.2	23.04170	121.10590	04.63	
08	2022	09	17	13	49	45.4	23.08904	121.15619	10.70	
09	2022	09	17	13	50	22.5	23.08776	121.14108	12.32	+
10	2022	09	17	13	50	46.1	23.07298	121.16299	08.88	
11	2022	09	17	13	51	14.0	23.04522	121.10281	06.59	
12	2022	09	17	13	51	24.2	23.02963	121.13734	08.38	
13	2022	09	17	13	51	47.6	23.09018	121.17395	07.67	
14	2022	09	17	13	52	43.0	23.03156	121.17955	04.39	+
15	2022	09	17	13	53	24.8	23.08111	121.18546	07.42	
16	2022	09	17	13	53	35.3	23.10270	121.16354	10.67	+
17	2022	09	17	13	54	16.0	23.09920	121.16238	07.80	
18	2022	09	17	13	54	43.4	23.07831	121.16753	09.83	+
19	2022	09	17	13	55	13.8	23.10737	121.14993	10.92	
20	2022	09	17	13	55	41.6	23.12378	121.16028	10.49	+
21	2022	09	17	13	57	01.9	23.09948	121.14798	07.16	+

Huang *et al. Terrestrial, Atmospheric and Oceanic Sciences* (2024) 35:1

Page 13 of 14

Table 2 (continued)

#	Year	m	d	h	mn	sec	lat	lon	dep	BPEQ[a]
22	2022	09	17	13	57	17.8	23.14071	121.15299	10.66	+
23	2022	09	17	13	58	20.2	23.14677	121.14967	10.89	+
24	2022	09	17	13	58	50.7	23.03436	121.23302	17.65	
25	2022	09	17	13	59	11.1	23.18617	121.15330	04.08	
26	2022	09	17	13	59	27.0	22.98787	121.06712	04.12	
27	2022	09	17	13	59	51.6	23.07656	121.16349	04.09	+
28	2022	09	17	14	00	18.3	23.06651	121.17497	11.73	
29	2022	09	17	14	00	45.5	23.12142	121.15077	10.87	+
30	2022	09	17	14	01	04.3	23.10794	121.14091	10.56	+
31	2022	09	17	14	01	15.0	23.14824	121.15579	11.67	+
32	2022	09	17	14	01	57.3	23.17870	121.15279	06.16	
33	2022	09	17	14	02	34.8	23.14763	121.15200	11.72	+
34	2022	09	17	14	03	43.6	23.04909	121.12793	11.04	
35	2022	09	17	14	04	14.7	22.99771	121.09299	09.54	+
36	2022	09	17	14	04	36.0	23.04638	121.10711	04.04	+
37	2022	09	17	14	05	25.9	23.01889	121.09670	06.54	+
38	2022	09	17	14	05	44.3	23.14195	121.15247	10.56	+
39	2022	09	17	14	06	48.4	23.04987	121.15099	07.76	+
40	2022	09	17	14	07	32.4	23.10076	121.16280	05.11	+
41	2022	09	17	14	07	44.3	23.12931	121.15334	10.68	+
42	2022	09	17	14	07	58.2	23.14762	121.15622	09.56	
43	2022	09	17	14	08	47.4	23.12301	121.16119	09.90	

In conclusion, results of this study indicate the importance of utilizing advanced imaging techniques like BP method to enhance the understanding of aftershock sequences and improve seismic hazard assessments. The results contribute to the knowledge of post-earthquake processes and can assist in refining seismic monitoring strategies for large events in the future.

Author contributions
B-SH carried out the calculations and drafted the manuscript. C-SK and C-JL supported to collect data, S-JL provided finite slip fault model and valuable suggestions, Y-LEC, J-SJ and W-FS have discussed deeply for data and interpretation. All authors read and approved the final manuscript.

Data availability
The authors thanks CWA for providing the TSMIP data (https://gdms.cwa.gov.tw/network_tsmip.php) and the broadband seismic data from BATS (https://bats.earth.sinica.edu.tw/).

Declarations

Competing interests
The authors declare that they have no competing interests.

References
Beskardes GD, Hole JA, Wang K, Michaelides M, Wu Q, Chapman MC, Davenport KK, Brown LD, Quiros DA (2018) A comparison of earthquake backprojection imaging methods for dense local arrays. Geophys J Int 212(3):1986–2002. https://doi.org/10.1093/gji/ggx520

Chen YL, Shin TC (1998) Study of the earthquake location of 3-D velocity structure in Taiwan area. Meteorol Bull 42:135–169

Gadallah M, Fisher R (2005) Applied seismology: a comprehensive guide to seismic theory and application. PennWell, USA, p 600

Gadallah M, Fisher R (2009) Exploration geophysics. Springer, Berlin, p 274

Gulia L, Rinaldi AP, Tormann T, Vannucci G, Enescu B, Wiemer S (2018) The effect of a mainshock on the size distribution of the aftershocks. Geophys Res Lett 45:13277–13287. https://doi.org/10.1029/2018GL080619

Huang BS (1996) A Fortran 77 Program to compute seismic rays travelling inside a radially inhomogeneous earth. Comput Geosci 22:287–303

Huang BS, Huang WG, Huang YL, Kuo LC, Chen KC, Angelier J (2009) Complex fault rupture during the 2003 Chengkung, Taiwan earthquake sequence from dense seismic array and GPS observations. Tectonophysics 466:184–204. https://doi.org/10.1016/j.tecto.2007.11.025

Huang CM, Chang LH, Kuo-Chen H, Zhuang Y (2023) SeisBlue: a deep-learning data processing platform for seismology, EGU General Assembly

Huang *et al. Terrestrial, Atmospheric and Oceanic Sciences* (2024) 35:1

Page 14 of 14

2023, Vienna, Austria, 24–28 Apr 2023, EGU23-13927. https://doi.org/10.5194/egusphere-egu23-13927.

Ishii M, Shearer PM, Houston H, Vidale JE (2005) Extent, duration and speed of the 2004 Sumatra-Andaman earthquake imaged by the Hi-Net array. Nature 435:933–936

Ishii M, Shearer PM, Houston H, Vidale JE (2007) Teleseismic P wave imaging of the 26 December 2004 Sumatra-Andaman and 28 March 2005 Sumatra earthquake ruptures using the Hi-net array. J Geophys Res 122:B11307. https://doi.org/10.1029/2006JB004700

Kiser E, Ishii M (2013) Hidden aftershocks of the 2011 M_w 9.0 Tohoku, Japan earthquake imaged with the backprojection method. J Geophys Res Solid Earth 118:5564–5576. https://doi.org/10.1002/2013JB010158

Klein FW (1978) Hypocenter location program Hypoinverse. U.S. Geol. Surv. Open- File Report. 78-694.

Klein FW (2003) The Hypoinverse2000 earthquake location program. In: Lee WHK, Kanamori H, Jennings PC, Kisslinger C (eds) International Handbook of Earthquake & Engineering Seismology, Part B. Academic Press, London (for International Association of Seismology and Physics of the Earth's Interior), p. 1619–1620

Kuo-Chen H, Sun W, Huang C, Pan S (2022) Near real-time seismic data processing helps scientist understand aftershocks, Temblor. https://doi.org/10.32858/temblor.276

Lahr JC (1989) Hypoellipse/Version 2.0: A computer program for determining local earthquakes hypocentral parameters, magnitude, and first motion pattern. U.S. Geological Survey Open-File Report 89-116, pp. 92

Lahr JC (2003) The Hypoellipse earthquake location program. In: Lee WHK, Kanamori H, Jennings PC, Kisslinger C (eds) International Handbook of Earthquake & Engineering Seismology, Part B. Academic Press, London (for International Association of Seismology and Physics of the Earth's Interior), pp. 1617–1618

Lee Y-H, Chen G-T, Rau R-J, Ching K-E (2008) Coseismic displacement and tectonic implication of 1951 Longitudinal Valley earthquake sequence, eastern Taiwan. J Geophys Res 113:B04305. https://doi.org/10.1029/2007JB005180

Lee SJ, Liu TY, Lin TC (2023) The role of the west-dipping collision boundary fault in the Taiwan 2022 Chihshang earthquake sequence. Sci Rep. 13:3552. https://doi.org/10.1038/s41598-023-30361-0

Lee WHK, Lahr JC (1975) HYPO71 (revised): a computer program for determining hypocenter, magnitude and first motion pattern of local earthquakes. U.S. Geological Survey Open-File Report 75-311, pp 116

Lee WHK, Lahr JC, Valdes CM (2003) The HYPO71 earthquake location program. In: Lee WHK, Kanamori H, Jennings PC, Kisslinger C (eds) International Handbook of Earthquake & Engineering Seismology, Part B. Academic Press, London (for International Association of Seismology and Physics of the Earth's Interior), pp. 1641–1642

Lienert BR, Havskov J (1995) A computer program for locating earthquakes both locally and globally. Seismol Res Lett 66(5):26–36

Lin CW, Liu YC, Chou PS, Lin YH (2021) Recent development of active fault investigations of Taiwan. Bull Centr Geol Surv 34:1–40

Meng L, Inbal A, Ampuero J-P (2011) A window into the complexity of the dynamic rupture of the 2011 Mw 9 Tohoku-Oki earthquake. Geophys Res Lett 38:L00G07. https://doi.org/10.1029/2011GL048118

Mozziconacci L, Delouis B, Huang BS, Lee JC, Béthoux N (2013a) Determining fault geometry from the distribution of coseismic fault slip related to the 2006 Taitung Earthquake, Eastern Taiwan. Bull Seisl Soc Am 103:394–411. https://doi.org/10.1785/0120110232

Mozziconacci L, Huang BS, Delouis B, Lee JC, Lee SJ (2013b) Rupture behavior of a Moderate earthquake (MW 5.9, April 2006) and its close relation with the 2003 Chengkung earthquake (Mw 6.8) at the Southern Termination of the plate boundary, Southeast Taiwan. J Asian Earth Sci 75:213–225. https://doi.org/10.1016/j.jseaes.2013.07.025

Roecker SW, Yeh YH, Tsai YB (1987) Three-dimensional P and S wave velocity structures beneath Taiwan—deep structure beneath an arc-continent collision. J Geophys Res 92:10547–10570

Shyu JBH, Sieh K, Chen YG, Chung LH (2006) Geomorphic analysis of the central range fault, the second major active structure of the Longitudinal Valley suture, eastern Taiwan. Geol Soc Am Bull 118:1447–1462. https://doi.org/10.1130/B25905.1

Shyu JBH, Chung LH, Chen YG, Lee JC, Sieh K (2007) Re-evaluation of the surface ruptures of the November 1951 earthquake series in eastern Tai- wan, and its neotectonic implications. J Asian Earth Sci 31:317–331. https://doi.org/10.1016/j.jseaes.2006.07.018

Sun W, Pan SY, Huang CM, Guan ZK, Yen IC, Ho CW, Chi TC, Ku CS, Huang BS, Fu CC, Kuo-Chen H (2023) Deep learning-based earthquake catalog reveals the rupture process of the 2022 Mw 6.9 Chihshang earthquake sequence, submitted to "Terrestrial, Atmospheric and Oceanic Sciences", Special issue of 2022 Eastern Taiwan Longitudinal Valley Earthquakes on August 29, 2023

Wen S, Wen YY, Ching KE, Yeh YL, Lee YH (2019) Tectonic implications on the 2018 Hualien Earthquake. Terr Atmos Ocean Sci 30:389–398. https://doi.org/10.3319/TAO.2019.01.28.01

Zhang Y, An Y, Long F, Zhu G, Qin M, Zhong Y, Xu Q, Yang H (2021) Short-term foreshock and aftershock patterns of the 2021 Ms 6.4 Yangbi Earthquake Sequence. Seismol Res Lett 93:21–32. https://doi.org/10.1785/0220210154

Publisher's Note